International Journal of Mass Spectrometry 280 (2009) 226–234

Contents lists available at ScienceDirect

International Journal of Mass Spectrometry

journal homepage: www.elsevier.com/locate/ijms

Reactions of Hf^+, Ta^+, and W^+ with O_2 and CO: Metal carbide and metal oxide cation bond energies

Christopher S. Hinton, Fengxia Li, P.B. Armentrout*

Chemistry Department, University of Utah, 315 South, 1400 East, Room 2020, Salt Lake City, UT 84112, United States

ARTICLE INFO

Article history:
Received 5 August 2008
Received in revised form 27 August 2008
Accepted 27 August 2008
Available online 7 September 2008

This article is dedicated to Zdenek Herman on the occasion of his 75th birthday and in recognition of his outstanding contributions to ion chemistry and the mass spectrometry community over many years.

Keywords:
Bond energy
Ionization energy
Transition metal carbide
Transition metal oxide
Thermochemistry

ABSTRACT

The reactions of Hf^+, Ta^+, and W^+ with O_2 and CO are studied as a function of translational energy in a guided ion beam tandem mass spectrometer. All three reactions with O_2 form diatomic metal oxide cations in exothermic reactions that occur at the collision rate. In the CO systems, formation of both diatomic metal oxide and metal carbide cations is observed to be endothermic. The energy-dependent cross sections in the latter systems are interpreted to give 0 K bond energies (in eV) of $D_0(HfC^+) = 3.19 \pm 0.03$, $D_0(TaC^+) = 3.79 \pm 0.04$, $D_0(WC^+) = 4.76 \pm 0.09$, $D_0(HfO^+) = 6.91 \pm 0.11$, $D_0(TaO^+) = 7.10 \pm 0.12$, and $D_0(WO^+) = 6.77 \pm 0.07$. The present experimental values for TaO^+ and WC^+ agree well with literature thermochemistry, those for HfO^+ and WO^+ refine the available literature bond energies, and those for HfC^+ and TaC^+ are the first measurements available. The nature of the bonding in MO^+ and MC^+ is discussed and compared for these three metal ions and analyzed using theoretical calculations at a B3LYP/HW+/6-311+G(3df) level of theory. Bond energies for all MO^+ and MC^+ species are calculated using geometries calculated at this level and single point energies determined at B3LYP, CCSD, CCSD(T), QCISD, and QCISD(T) levels of theory with the same basis set. Reasonable agreement between the theoretical and experimental bond energies for the three metal oxide and three metal carbide cations is found. Potential energy surfaces for reaction of the metal cations with CO are also calculated at the B3LYP level of theory and reveal additional information about the reaction mechanisms.

1. Introduction

Transition metal carbides and oxides play an important role in many processes. Because of their high melting point, conductivity, and hardness, transition metal carbides play important roles in material science and electronics [1–3]. The oxides of transition metals play vital roles in industrial, organometallic, and atmospheric chemistry [4–6]. In understanding the origins of these important properties, it can be useful to understand the binding of the simplest examples of such species. In previous studies in our laboratory, guided ion beam mass spectrometry has been used to systematically study diatomic oxides, MO^+, and carbides, MC^+, of first-row [7,8], second-row [9–11], and third-row [12] transition metal cations. In the present work, these studies are extended to include the group 4–6 third-row transition metal cations, M = Hf, Ta, and W. The comparison of the metal carbides and oxides is interesting because both C and O have two unpaired valence electrons in their ^3P ground states, easily making two covalent bonds to metals. However, the empty p orbital on C versus the doubly occupied p orbital on oxygen can make an appreciable difference in the bonding of these species with metals.

The guided ion beam methods used in our laboratory can be used to investigate the bond dissociation energies (BDEs) for M^+–O and M^+–C species by analyses of the kinetic energy dependence of reactions (1)–(3).

$$M^+ + O_2 \rightarrow MO^+ + O \quad (1)$$

$$M^+ + CO \rightarrow MO^+ + C \quad (2)$$

$$M^+ + CO \rightarrow MC^+ + O \quad (3)$$

In previous work [7–11], it has been shown that the early transition metal cations (groups 3–5) react exothermically with O_2, whereas later transition metal cations (groups 6–11) react endothermically. To obtain metal oxide bond energies for these early metal cations, reactions with CO, which has a much stronger bond, $D_0(CO) = 11.108$ eV versus $D_0(O_2) = 5.115$ eV [13], can be used as now the processes are endothermic. Furthermore, the competing formation of MC^+ in reaction (3) is also observed, such that analyses of the energy-dependent cross section data for reactions (2) and (3) allow 0 K metal oxide and metal carbide BDEs to be obtained. Detailed theoretical calculations are also performed here in order

* Corresponding author. Tel.: +1 801 581 7885; fax: +1 801 581 8433.
E-mail address: armentrout@chem.utah.edu (P.B. Armentrout).

1387-3806/$ – see front matter © 2008 Elsevier B.V. All rights reserved.
doi:10.1016/j.ijms.2008.08.025

to provide information regarding the electronic states of the MC^+ and MO^+ species and to examine the potential energy surfaces for formation of the products in reactions (2) and (3).

2. Literature data

Literature information on thermodynamics of these transition metal oxide and carbide species is generally sparse, although all three metal oxides have been studied by Knudsen effusion techniques. Panish and Reif used Langmuir vaporization and Knudsen effusion to measure the 0 K dissociation energy of HfO as 7.92 ± 0.26 eV [14], and later Ackermann and Rauh measured a value of 8.19 ± 0.09 eV [15]. Pedley and Marshall critically evaluate these values and select $D_0(\mathrm{HfO}) = 8.26 \pm 0.13$ eV [16]. In contrast, an RKR analysis of spectroscopic information suggests that $D_0(\mathrm{HfO}) = 9.04 \pm 0.02$ eV [17], but this value is less reliable because of the long range extrapolation involved. Using Eq. (4),

$$D_0(\mathrm{M-X}) + \mathrm{IE(M)} = D_0(\mathrm{M^+ - X}) + \mathrm{IE(MX)} \quad (4)$$

the ionization energy of this species, $\mathrm{IE(HfO)} = 7.55 \pm 0.1$ eV, measured by Rauh and Ackermann [18], and $\mathrm{IE(Hf)} = 6.825$ eV [19] can be combined with the best neutral BDE to yield $D_0(\mathrm{Hf^+–O}) = 7.54 \pm 0.16$ eV. The review of transition metal oxide cations by Schroder et al. [20] lists $D(\mathrm{Hf^+–O}) = 7.50 \pm 0.22$ eV and cites the GIANT (Gas-phase Ion And Neutral Thermochemistry) compilation [21], which used the same reference data for HfO but an older value for $\mathrm{IE(Hf)} = 6.78$ eV. ESR studies [22] identify HfO^+ as having a $^2\Sigma$ ground state and a variety of spectroscopic studies of HfO [23–25] have also been performed.

For tantalum oxide, the JANAF tables [26] discuss the large disparities obtained by several Knudsen cell mass spectrometry studies [27–29]: 2nd and 3rd law values for $\Delta_f H_{298}(\mathrm{TaO})$ values ranging from 2.14 to 4.35 eV. After correlating values with those for the 1st and 2nd row congeners, VO and NbO, Chase chooses a rounded value from a Birge–Sponer extrapolation corrected for iconicity, $\Delta_f H_{298}(\mathrm{TaO}) = 1.99_5 \pm 0.65$ eV and $D_0(\mathrm{TaO}) = 8.65 \pm 0.65$ eV. Pedley and Marshall [16] primarily utilize results from Smoes et al. [30] and select $D_0(\mathrm{TaO}) = 8.24 \pm 0.13$ eV. The situation for the ionization energy of TaO is equally unclear. The most precise and most recent value comes from a photoelectron measurement of Dyke et al., 8.61 ± 0.02 eV [31], which is well above previous electron impact measurements of $7.9_2 \pm 0.1$ eV from Ackermann et al. [32] and 7.5 ± 0.5 eV from Smoes et al. [30]. Combining the best values presently available with $\mathrm{IE(Ta)} = 7.5495$ eV [33] yields $D_0(\mathrm{Ta^+–O}) = 7.18 \pm 0.14$ eV. The review by Schroder et al. [20] lists $D(\mathrm{Ta^+–O}) = 8.15 \pm 0.65$ eV, again citing the GIANT compilation [21], which uses older values for $\mathrm{IE(Ta)} = 7.4$ eV and $\mathrm{IE(TaO)} = 7.92$ eV, along with $D_0(\mathrm{TaO}) = 8.65$ eV. Additional work has examined the spectroscopy of TaO, identifying its ground state as $^2\Delta$ [34–38], and has characterized the photoelectron spectrum of TaO^- [39].

Finally, the JANAF tables [26] reanalyzed the Knudsen cell mass spectrometry data of DeMaria et al. [40] to determine $\Delta_f H_0(\mathrm{WO}) = 4.41 \pm 0.43$ eV, which can be combined with the heats of formation of W and O (also taken from JANAF) to give $D_0(\mathrm{WO}) = 6.95 \pm 0.44$ eV, somewhat higher than the value quoted directly by DeMaria et al. of 6.68 ± 0.44 eV. (Also, using $H_{298} - H_0$ data taken from the JANAF tables, one finds that $D_{298}(\mathrm{W–O}) - D_0(\mathrm{W–O}) = 0.043$ eV, yielding $D_{298}(\mathrm{WO}) = 7.00 \pm 0.44$ eV.) Pedley and Marshall use the same data to select $D_0(\mathrm{WO}) = 6.92 \pm 0.44$ eV. DeMaria et al. also quote a rough ionization energy for WO of 9.1 ± 1 eV, but recent gas-phase bracketing studies by Bohme and co-workers have refined this greatly to 8.1 ± 0.3 eV [41]. When combined with $\mathrm{IE(W)} = 7.864$ eV [42] and $D_0(\mathrm{WO}) = 6.92 \pm 0.44$ eV, this IE value yields $D_0(\mathrm{W^+–O}) = 6.68 \pm 0.53$ eV. This value is well above that quoted in the review by Schroder et al. [20] who list $D(\mathrm{W^+–O}) = 5.46 \pm 0.43$ eV as taken from the GIANT compilation [21]. Bohme and co-workers verified the accuracy of their cation bond energy by determining that W^+ reacts at room temperature with COS to form WO^+, albeit with an efficiency of only 0.38. They took this to indicate that $D_{298}(\mathrm{W^+–O}) > D_{298}(\mathrm{O–CS}) = 6.85 \pm 0.04$ eV (although the inefficiency of this reaction could mean that these bond energies are nearly isoenergetic). They then combined this limit with $D_{298}(\mathrm{W^+–O}) = 6.81 \pm 0.82$ eV (which is slightly higher than the value derived above for reasons that are unknown and with an uncertainty determined by addition of the literature uncertainties rather than combining them in quadrature) to yield a refined range of values that is cited as $D_{298}(\mathrm{W^+–O}) = 7.20 \pm 0.43$ eV. This value is then combined with the ionization energies of W and WO to determine a value for $D_{298}(\mathrm{W–O})$ as 7.46 ± 0.74 eV, or equivalently $D_0(\mathrm{W–O}) = 7.42 \pm 0.74$ eV, consistent with the JANAF and Pedley and Marshall values within the broad uncertainties. Spectroscopic work [43,44] has identified the ground state of WO as $X^3\Sigma^-$.

For the carbide of Hf, we could find no literature reports of gas-phase studies. A number of neutral [45] and cationic [46,47] tantalum carbide clusters formed by laser vaporization have been studied. On the basis of the observation of several reactions involving TaC^+, McElvany and Cassady were able to bracket its bond energy as $3.38 \text{ eV} < D(\mathrm{TaC^+}) < 6.11$ eV. Furthermore, Majumdar and Balasubramanian have studied this molecule and its neutral analogue theoretically [48,49]. For tungsten, spectroscopy has identified the ground state of WC as $^3\Delta$ [50]. The photoelectron spectrum of WC^- has been measured [51], and establishes the electron affinity of WC as well as the excitation energies for several excited states of this molecule. In addition, WC^+ has been observed as a product in the reaction of W^+ with CH_4 [52]. Measurement of the endothermic threshold for this double dehydrogenation reaction determined the 0 K bond energy of WC^+ as 4.96 ± 0.22 eV. WC^+ has also been observed in the fragmentation of $W(CO)_6$ ionized by electron impact [53] and by photoionization [54], and in the photoionization of W(CO) [55]. The appearance energies obtained in these studies suggest that $D_0(\mathrm{W^+–C}) = 5.26 \pm 0.78$, 3.93 ± 0.36, and 3.86 ± 0.35 eV, respectively. Finally, we note that Musaev et al. have examined the WCO^+ system theoretically, exploring the potential energy surface for activation of the CO molecule by W^+ [56].

3. Experimental

3.1. General procedures

The guided ion beam tandem mass spectrometer on which these experiments were performed has been described in detail previously [57]. Ions are generated in a direct current discharge flow tube (DC/FT) source described below [58]. The ions are extracted from the source, accelerated, and focused into a magnetic sector momentum analyzer for mass selection of primary ions, where either the ^{180}Hf isotope (35.2% natural abundance), the ^{181}Ta isotope (99.99% natural abundance), or ^{186}W isotope (30.67% natural abundance) are selected. The mass selected ions are then slowed to a desired kinetic energy and focused into an octopole ion guide that radially traps the ions [59]. The octopole passes through a static gas cell that contains the neutral reaction partner at a low pressure (ranging from 0.05 to 0.2 mTorr) so that multiple ion–molecule collisions are improbable. All results reported here result from single bimolecular encounters, as verified by the independence of the measured cross sections on the neutral reactant pressure. Product and remaining reactant ions are contained in the guide until

they drift to the end of the octopole, where they are focused and extracted into a quadrupole mass filter for mass analysis and then detected. Reaction cross sections are calculated from product ion intensities relative to reactant ion intensities after correcting for background signals [60]. Uncertainties in the absolute cross sections are estimated to be ±20%.

Laboratory ion energies (lab) are converted to energies in the center-of-mass frame (CM) by using the formula, $E_{CM} = E_{lab}\, m/(m+M)$, where M and m are the ion and neutral masses, respectively. Two effects broaden the cross section data: the kinetic energy distribution of the ion and the thermal motion of the neutral reactant gas (Doppler broadening) [61]. The absolute zero and the full width at half-maximum (fwhm) of the kinetic energy distribution of the reactant ions are determined by using the octopole beam guide as a retarding potential analyzer. The distributions of ion energies are independent of energy, nearly Gaussian, and have typical fwhm of 0.6–1.4 eV (lab). Uncertainties in the absolute energy scale are ±0.05 eV (lab).

3.2. Ion source

M^+ ions are produced in a DC/FT source, consisting of a cathode held at a high negative voltage (1.1–1.5 kV) over which a flow of approximately 90% He and 10% Ar passes at a total pressure of 0.3–0.5 Torr. The dc-discharge is used to ionize Ar and then accelerate these ions into a cathode either made of tantalum or iron with a cavity containing hafnium or tungsten metal. After the ions are swept down a meter-long flow tube, they undergo ~10^5 thermalizing collisions with He and Ar. No evidence for low-lying excited states of the three metal ions (such as cross section features having lower energy thresholds) within about 1% sensitivity is observed under these flow conditions. When compared to a surface ionization source, the DC/FT source has been found to generate Sc^+ [62], Fe^+ [63], Co^+ [64], Ni^+ [65], Ru^+ [66], Rh^+ [66], and Pd^+ [66] ions with an average electronic temperature of 700 ± 400 K, and Y^+, Zr^+, Nb^+, and Mo^+ ions with an average electronic temperature of 300 ± 100 K [67]. Even at the maximum electronic temperature of 1100 K, the three metal ions populate the lowest energy spin–orbit level to a high degree as shown in Table S1, which lists the various low-lying states of Hf^+ [68], Ta^+ [69], and W^+ [70]. Conservatively, the average electronic energy, E_{el}, at a temperature of 700 ± 400 K for Hf^+ is 0.006 + 0.010/−0.006 eV, for Ta^+ is 0.025 + 0.039/−0.023 eV, and for W^+ is 0.018 + 0.040/−0.018 eV.

3.3. Data analysis

The cross sections of the endothermic reactions are modeled using Eq. (5) [71–74],

$$\sigma(E) = \frac{\sigma_0 \sum_i g_i (E + E_i + E_{rot} - E_0)^n}{E} \quad (5)$$

where σ_0 is an energy-independent scaling factor, E is the relative kinetic energy of the reactants, n is an adjustable parameter that characterizes the energy dependence of the process [71], E_{rot} is the rotational energy of the diatomic reactant (=k_BT at 300 K = 0.026 eV), and E_0 is the 0 K threshold for reaction of electronic, vibrational, and rotational state reactants. The model involves an explicit sum of the contributions of individual electronic states of the M^+ reactant, denoted by i, having energies E_i and populations g_i. Before comparison with the experimental data, Eq. (5) is convoluted with the kinetic energy distributions of the reactant ions and neutral reactants at 300 K. The σ_0, n, and E_0 parameters are then optimized using a nonlinear least-squares analysis to give the best reproduction of the data [71,73]. Error limits for E_0 are calculated from the range of threshold values for different data sets over a range of acceptable n values (as specified in the table of fitting parameters given below) combined with the absolute errors in the kinetic energy scale and internal energies of reactant ions.

At higher energies, the cross sections decline because the product ions have sufficient energy to dissociate. In this high-energy region, the data can be modeled by modifying Eq. (5) to include the dissociation probability according to a statistical model discussed elsewhere [75]. This probability is controlled by two parameters: p, which is an adjustable parameter similar to n, and E_d, which is the energy at which product ions start decomposing. In this study, the values of p and E_d are allowed to vary (although p can only hold integral values) and used to fit cross sections of M^+ with CO. Use of this high-energy model does not alter significantly the analysis of the threshold regions.

3.4. Theoretical calculations

Quantum chemistry calculations reported here were computed using the B3LYP hybrid density functional method [76,77] and performed with the GAUSSSIAN 03 suite of programs [78]. The 6-311+G(3df) basis set, triple zeta with diffuse and polarization functions, was used for carbon and oxygen in all calculations. As a point of comparison, the single point bond energies for O–O and C–O are calculated as 5.279 and 11.059 eV (uncorrected for spin–orbit coupling) compared to the experimental values of 5.115 and 11.108 eV [13], respectively.

The core electrons of hafnium, tantalum, and tungsten are described by the relativistic effective core potentials (ECP) of Hay-Wadt (HW) [79], with valence electrons described by the Los Alamos double zeta basis set (LANL2DZ). This basis set is optimized for neutral atoms, whereas the positive charge of the metal ion differentially contracts the s orbitals compared to the d orbitals. Therefore, calculations were performed with an altered HW-ECP basis set for the metal ions as described by Ohanessian et al. (designated as HW^+) [80]. The calculated thermochemistry is then corrected for zero point energy effects, after scaling the frequencies by 0.9804 [81]. Single point energies were also calculated from the B3LYP optimized geometries at QCISD, CCSD, QCISD(T), and CCSD(T) levels using the same basis sets. No corrections for spin–orbit coupling are included in the theoretical values, as discussed further below.

4. Results

4.1. Hf^+, Ta^+, and $W^+ + O_2$

Fig. 1 shows the cross sections of reaction (1) for $M^+ = Hf^+$, Ta^+, and W^+ as a function of kinetic energy. The HfO^+, TaO^+, and WO^+ cross sections decrease with increasing kinetic energy, consistent with the behavior of exothermic ion–molecule reactions. This behavior can be described using the Langevin–Gioumousis–Stevenson (LGS) model [82], Eq. (6),

$$\sigma_{LGS} = \pi e \left(\frac{\alpha}{2\pi\varepsilon_0 E} \right)^{1/2} \quad (6)$$

where e is the charge on the electron, α is the polarizability volume of the neutral reactant molecule (1.57 Å^3 for O_2) [83], and ε_0 is the permittivity of vacuum. As can be seen from Fig. 1, the cross sections for all three metal ions have energy dependences of $E^{-0.5\pm0.1}$ at energies below about 1 eV, as predicted by σ_{LGS}. The magnitudes of the cross sections obtained for the reactions are approximately equivalent to that of σ_{LGS} in this energy range (within the 20% absolute uncertainty), indicating that the reactions occur with 100 ± 20% efficiency. We can also convert this cross section into a room temperature rate constant using methods outlined previously

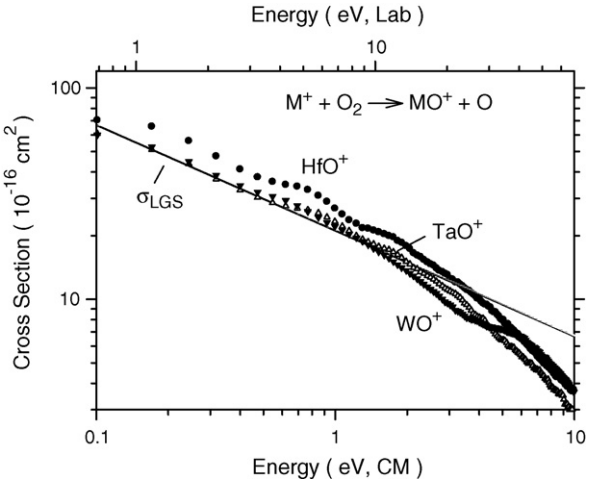

Fig. 1. Cross sections for reactions of Hf^+ (solid circles), Ta^+ (open triangles), and W^+ (solid inverted triangles) with O_2 as a function of kinetic energy in the center-of mass frame (lower *x*-axis) and laboratory frame (upper *x*-axis) for $M^+ = Hf^+$. The line shows the calculated collision cross section, σ_{LGS}.

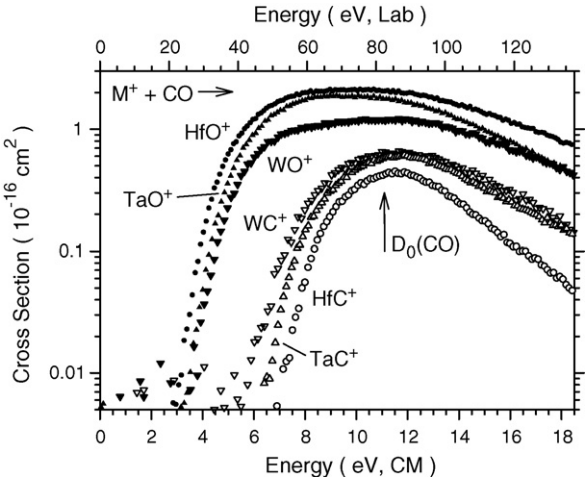

Fig. 2. Cross sections for reactions of Hf^+ (circles), Ta^+ (triangles), and W^+ (inverted triangles) with CO to form metal oxide (solid symbols) and metal carbide (open symbols) cation products as a function of kinetic energy in the center-of mass frame (lower *x*-axis) and laboratory frame (upper *x*-axis) for $M^+ = Hf^+$.

[57]. For Hf^+, Ta^+, and W^+, this yields rate constants of (6.9 ± 1.5), (6.1 ± 1.2), and $(6.0 \pm 1.2) \times 10^{-10}$ cm^3 molecule^{-1} s^{-1}, respectively, compared to $k_{LGS} = 5.6 \times 10^{-10}$ cm^3 molecule^{-1} s^{-1}. These values can be compared favorably with the rate constants measured by Bohme and co-workers in 0.35 Torr of helium at 295 K (4.1 ± 1.2), (4.7 ± 1.4), and $(4.4 \pm 1.3) \times 10^{-10}$ cm^3 molecule^{-1} s^{-1} [84], respectively, corresponding to reaction efficiencies of 67 ± 20, 82 ± 25, and 79 ± 24%. The present values agree with these within experimental uncertainties although the high-pressure rate constants are systematically lower than the present single collision values for reasons that are unclear. However, it is notable that among the 29 transition metal ions examined in this work, the highest reaction efficiency observed was 82% (for Ta^+ and Zr^+), although there is no obvious reason why some of these metal cations could not react on every collision.

Above about 1 eV, the cross sections begin to decrease more rapidly. This effect can be attributed to angular momentum conservation restraints, as previously discussed in detail [85,86]. This argument recognizes that because the reduced mass of the products of reaction (1), μ', is smaller than that of the reactants, μ (μ'/μ is approximately 1/2 in these systems), the centrifugal barrier in the product channel can exceed that in the reactant channel for large angular momenta. This restricts the probability of reaction at higher kinetic energies. We have previously outlined a simple model to predict where these angular momentum constraints can restrict the product formation in exothermic reactions [86]. This begins at an energy given by Eq. (7),

$$E_C = \frac{(E - \Delta H)(\alpha' \mu'^2)}{(\alpha \mu^2)} \quad (7)$$

where α and α' are the polarizability volumes of the reactant and product neutrals (1.57 and 0.80 Å^3, respectively) [83,87], E is the relative kinetic energy of the reactants, and ΔH is the enthalpy of reaction. Using thermochemistry obtained below for HfO^+, TaO^+, and WO^+, this model predicts that the HfO^+, TaO^+, and WO^+ cross sections will become constrained beginning at 0.32, 0.35, and 0.29 eV, respectively, in reasonable agreement with the data.

We also observed HfO_2^+, TaO_2^+, and WO_2^+ at the lowest kinetic energies, products that are formed by secondary reactions of the primary MO^+ products, as verified by the dependence of the metal dioxide cation product cross sections on O_2 pressure. The kinetic energy dependences of the cross sections of these products are also consistent with the secondary reactions, $MO^+ + O_2 \rightarrow MO_2^+ + O$, and demonstrate that they are exothermic for all three metals.

4.2. Hf^+, Ta^+, and $W^+ + CO$

Cross sections for reactions (2) and (3) are shown in Fig. 2. The MO^+ cross sections rise from apparent thresholds of 3–4 eV, whereas the MC^+ cross sections require more energy, rising from thresholds of 5–7 eV. It can be seen that the relative ordering of the thresholds is inverted between the oxide and carbide ion products, with Hf^+ having the lowest oxide threshold and the highest carbide threshold, whereas W^+ has the highest oxide and lowest carbide thresholds. This should directly reflect the relative bond dissociation energies of these product ions. Both MC^+ and MO^+ cross sections reach maxima near 11 eV because both product ions can dissociate further in reaction (8),

$$M^+ + CO \rightarrow M^+ + C + O \quad (8)$$

which has a thermodynamic threshold of 11.108 eV = D_0(CO) [13].

5. Thermochemical and theoretical results

5.1. Thermochemistry

The exothermic reactions (1) for $M^+ = Hf^+$, Ta^+, and W^+ provide only lower limits to the HfO^+, TaO^+, and WO^+ BDEs, $D_0(M^+–O) \geq D_0(O_2) = 5.115$ eV [13]. Therefore, in order to determine the M^+—O bond strengths, the reactions of Hf^+, Ta^+, and W^+ with CO are used to determine the BDEs more precisely. If there are no reaction barriers in excess of the reaction endothermicities, as is often the case for ion–molecule reactions, then the BDEs of M^+–O and M^+–C can be derived from the E_0 thresholds of reactions (2) and (3) by using Eqs. (9) and (10), respectively. If such barriers did exist, then the bond energies derived would be lower limits to the true thermodynamic values, but the quantum chemical calculations on the potential energy surfaces detailed below verify the veracity of this assumption in the present cases.

$$D_0(M^+–O) = D_0(C–O) – E_0(MO^+) \quad (9)$$

$$D_0(M^+–C) = D_0(C–O) – E_0(MC^+) \quad (10)$$

The endothermic cross sections for reactions (2) and (3) were analyzed with Eq. (5). The optimized fitting parameters are listed in

Table 1
Fitting parameters of Eq. (5) used to model reactions (2) and (3)[a]

Reactant	Product	σ_0	n	E_0 (eV)	$D_0(M^+–A)$
Hf^+	HfO^+	2.39 (0.56)	1.4 (0.1)	4.20 (0.11)	6.91 (0.11)
Ta^+	TaO^+	3.14 (0.62)	1.2 (0.2)	4.01 (0.12)	7.10 (0.12)
W^+	WO^+	1.87 (0.28)	1.3 (0.1)	4.34 (0.07)	6.77 (0.07)
Hf^+	HfC^+	1.70 (0.06)	1.0 (0.1)	7.92 (0.03)	3.19 (0.03)
Ta^+	TaC^+	1.64 (0.13)	1.0 (0.1)	7.32 (0.04)	3.79 (0.04)
W^+	WC^+	0.88 (0.18)	1.4 (0.1)	6.35 (0.09)	4.76 (0.09)

[a] Uncertainties, in parentheses, are one standard deviation.

Table 1 and typical reproduction of the data is shown in Fig. 3. This includes the high-energy analysis that accounts for reaction (8) above 11 eV.

Analysis of reactions (2) yields thresholds (Table 1) leading to metal oxide bond energies of 6.91 ± 0.11, 7.10 ± 0.12, and 6.77 ± 0.07 eV for HfO^+, TaO^+, and WO^+, respectively. The former value is outside of the combined experimental uncertainties from the cationic BDE in the literature, 7.54 ± 0.16 or 7.50 ± 0.22 eV [20] (Table 2). We believe this is because the ionization energy of HfO measured by Ackermann and Rauh, IE(HfO) = 7.55 ± 0.1 eV [15], is probably too low, as found independently for TaO. Ackermann and Rauh determined IE(TaO) = 7.92 ± 0.1 eV, whereas a photoelectron spectrum by Dyke et al. yields 8.61 ± 0.02 eV [31], a discrepancy of 0.7 ± 0.1 eV. In the case of HfO, combining our cationic bond energy with the neutral bond energy of Pedley and Marshall [16], D_0(Hf–O) = 8.26 ± 0.13 eV, we derive IE(HfO) = 8.18 ± 0.17 eV (Table 3), 0.63 ± 0.20 eV higher than the previous value, a comparable discrepancy to that found for TaO. Equivalently, the IEs of HfO and TaO measured by Ackermann and Rauh differ by 0.4 eV, which is the same relationship as our revised IE(HfO) compared to IE(TaO) from Dyke et al..

In the tantalum oxide system, our cationic BDE of 7.10 ± 0.12 eV agrees very well with the best value presently in the literature, $D_0(Ta^+–O) = 7.18 \pm 0.14$ eV (Table 2). If we combine our cationic BDE with IE(TaO) = 8.61 ± 0.02 eV from Dyke et al. [31], we obtain D_0(Ta–O) = 8.16 ± 0.12 eV (Table 3), very similar to the value selected by Pedley and Marshall of 8.24 ± 0.13 eV [16].

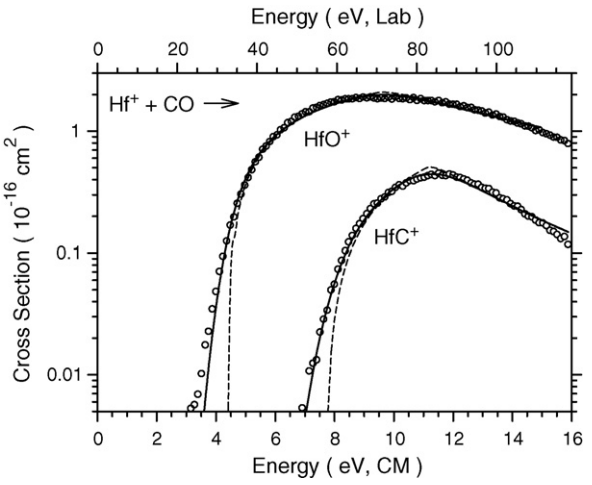

Fig. 3. Cross sections for formation of HfO^+ and HfC^+ in the reaction of Hf^+ with CO as a function of kinetic energy in the center-of-mass frame (lower x-axis) and laboratory frame (upper x-axis). Symbols indicate the experimental results. Dashed lines show the low energy model cross sections given by Eq. (5) and the parameters given in Table 1 along with a model for the dissociation of the product ions in reaction (8) at higher energies. Solid lines show these models convoluted over the experimental energy distributions.

For the tungsten oxide system, our measured BDE of 6.77 ± 0.07 eV is in very good agreement with the literature range determined using D_0(W–O) = 6.92 ± 0.44 eV from Pedley and Marshall [16] and IE(WO) = 8.1 ± 0.3 eV from Bohme and co-workers [41], $D_0(W^+–O) = 6.68 \pm 0.53$ eV (Table 2). Our value is also consistent with the observation of Bohme and co-workers that W^+ reacts at room temperature with COS to form WO^+. Bohme and co-workers interpreted this to mean that $D_{298}(W^+–O) \geq D_{298}$(O–CS) = 6.85 ± 0.04 eV, which is equivalent to $D_0(W^+–O) \geq 6.81 \pm 0.04$ eV, within experimental error of the present value. In this system, by combining our cation BDE with IE(WO) = 8.1 ± 0.3 eV [41], we refine the neutral BDE to D_0(W–O) = 7.01 ± 0.31 eV, consistent with but more precise

Table 2
Bond Dissociation Energies at 0 K[a]

Bond	Experiment		Theory					
	This work	Literature	B3LYP	QCISD(T)	CCSD(T)	QCISD	CCSD	Literature
O—O		5.115 ± 0.002[b]	5.279	4.929	4.914	4.627	4.954	
C—O		11.108 ± 0.005[b]	11.059	10.916	10.897	10.625	10.576	
Hf^+—O	6.91 ± 0.11	7.54 ± 0.16[c], 7.50 ± 0.22[d]	7.21	7.54	7.49	7.13	7.04	
Hf^+—C	3.19 ± 0.03		3.67	3.51	3.48	3.30	3.25	
Ta^+—O	7.10 ± 0.12	7.18 ± 0.14[e], 8.15 ± 0.65[d]	7.28	7.84	7.76	7.36	7.22	
Ta^+—C	3.79 ± 0.04	3.38–6.11[f]	4.48	4.79	4.88	4.72	4.32	4.50[g]
W^+—O	6.77 ± 0.07	6.68 ± 0.53[h], 7.16 ± 0.43[i] $\geq 6.81 \pm 0.04$[i], 5.46 ± 0.43[d]	6.92	7.11	6.96	6.78	6.60	
W^+—C	4.76 ± 0.09	4.96 ± 0.22[j], 3.93 ± 0.36[k] 3.86 ± 0.35[l], 5.26 ± 0.78[m]	4.88	4.34	4.39	4.81	4.57	
MAD			0.32	0.58	0.53	0.26	0.20	

[a] From this work, except as noted.
[b] Huber and Herzberg [13].
[c] Derived from references [16–19] and Eq. (4), see text.
[d] Schroder et al. [20].
[e] Derived from references [16,31,33] and Eq. (4), see text.
[f] Cassady and McElvany [46,47].
[g] Majumdar and Balasubramanian [48].
[h] Derived from references [16], [41], and [42] and Eq. (4), see text.
[i] Blagojevic et al. [41].
[j] Armentrout et al. [52].
[k] Qi et al. [54].
[l] Qi et al. [55].
[m] Winters and Kiser [53].

Table 3
Experimental thermochemical data for third row transition metal oxides

M^+–X	IE(M)	$D_0(M^+–X)$	D_0(M–X)		IE(MX)	
		This work	Literature	This work	Literature	This work
Hf^+–O	6.825[a]	6.91 ± 0.11	8.26 ± 0.13[b]		7.55 ± 0.1[c]	8.18 ± 0.17[d]
Ta^+–O	7.5495[e]	7.10 ± 0.12	8.24 ± 0.13[b]	8.16 ± 0.12[d]	8.61 ± 0.02[f], 7.92 ± 0.1[g], 7.5 ± 0.5[h]	8.69 ± 0.18[d]
W^+–O	7.864[i]	6.77 ± 0.07	6.92 ± 0.44[b], 6.95 ± 0.44[j]	7.01 ± 0.31[d]	8.1 ± 0.3[k], 9.1 ± 1[l]	8.04 ± 0.45[d]

[a] Callender et al. [19].
[b] Pedley and Marshall [16].
[c] Rauh and Ackermann [18].
[d] Derived from $D_0(MX) + IE(M) = D_0(MX^+) + IE(MX)$.
[e] Simard et al. [33].
[f] Dyke et al. [31].
[g] Ackermann et al. [32].
[h] Smoes et al. [30].
[i] Campbell-Miller and Simard [42].
[j] JANAF tables [26].
[k] Blagojevic et al. [41].
[l] DeMaria et al. [40].

than the literature values of 6.92 ± 0.44 [16] or 6.95 ± 0.44 eV [26].

As noted above, there is no literature thermochemistry for HfC^+ and only very broad limits are available for TaC^+, 3.38 eV < $D(TaC^+)$ < 6.11 eV [46,47]. Our much more precise value of $D_0(Ta^+–C)$ = 3.79 ± 0.04 eV lies within these limits. For WC^+, the 0 K BDE derived from analysis of reaction (3) is 4.76 ± 0.09 eV, within experimental uncertainty of the 4.96 ± 0.22 eV value obtained from the $W^+ + CH_4$ reaction system [52]. A weighted average of the two values from our laboratory is $D_0(W^+–C)$ = 4.80 ± 0.08 eV, which we take as our best determination in this system. This value lies in between those derived from the appearance energies of WC^+ and W^+ observed in the photoionization of $W(CO)_6$ and W(CO), 3.93 ± 0.36 and 3.86 ± 0.35 eV, respectively [54,55], and that derived from electron impact of $W(CO)_6$, 5.26 ± 0.78 eV [53]. The latter value agrees with the determinations from this laboratory within the large uncertainty. The low values from photoionization can probably be attributed to the failure to account for kinetic shifts in the tight (for formation of WC^+) versus loose (for formation of W^+) transition states associated with these dissociation processes.

5.2. Theoretical results: Metal oxide cations

Qualitatively, the bonding in transition metal oxides has been discussed at length by Schroder et al. [20]. The valence orbitals are 1σ (largely O 2s), 2σ (metal–oxygen sigma bonding), 1π (metal–oxygen pi bonding), 1δ (metal 5d nonbonding), 3σ (largely metal 6s5d hybrid), 2π (metal–oxygen pi antibonding), and 4σ (metal–oxygen sigma antibonding). Configuration interaction between the 1σ and 2σ orbitals could drive the 2σ above the 1π, and the relative order of the 1δ and 3σ nonbonding orbitals is also unclear. For HfO^+, there are nine valence electrons, suggesting an electron configuration of $1\sigma^2 2\sigma^2 1\pi^4 1\delta^1$ with a predicted $^2\Delta$ ground state or $1\sigma^2 2\sigma^2 1\pi^4 3\sigma^1$ with a $^2\Sigma^+$ ground state. The present calculations find the latter is the ground state with the $^2\Delta$ state lying 0.90 eV higher in energy (Table S2). This is consistent with the ground state determined by ESR spectroscopy [22]. These states have similar bond lengths of 1.701 and 1.714 Å, respectively. Other excited states necessarily remove an electron from one of the bonding orbitals (2σ or 1π) such that they lie 2.9 eV or more above the ground state and have appreciably longer bonds (1.84–1.95 Å) (Table S2).

Addition of another electron in TaO^+ suggests possible ground states of $^3\Delta$ ($1\sigma^2 2\sigma^2 1\pi^4 3\sigma^1 1\delta^1$), $^3\Sigma^-$ ($1\sigma^2 2\sigma^2 1\pi^4 1\delta^2$), or possibly $^1\Sigma^+$ ($1\sigma^2 2\sigma^2 1\pi^4 3\sigma^2$). Indeed, the present calculations find a $^3\Delta$ ground state, with the lowest energy excited state being the singlet-coupled version of this state, $^1\Delta$ having the same electron configuration (Table S2). The $^1\Sigma^+$ state was located 0.82 eV higher in energy. The $^3\Sigma^-$ state lies at 0.86 eV, whereas the singlet-coupled version of this state was found 1.07 eV above the ground state. All other excited states involve excitations out of the bonding orbitals and therefore lie over 3.4 eV higher in energy than the ground state. All low-lying states have bond lengths near 1.67 Å, whereas the higher lying excited states have longer bonds (1.86–1.88 Å), consistent with a lower bond order.

For WO^+, the obvious ground state is now $^4\Sigma^-$ ($1\sigma^2 2\sigma^2 1\pi^4 3\sigma^1 1\delta^2$) and indeed this is found to be the ground state computationally. Low-lying excited states include the low-spin coupled version of this state, $^2\Sigma^-$ having the same electronic configuration, and $^2\Delta$ ($1\sigma^2 2\sigma^2 1\pi^4 3\sigma^2 1\delta^1$). These states lie 0.84 and 1.47 eV above the ground state and all three states have bond lengths of 1.64–1.65 Å. Somewhat higher in energy are two $^4\Pi$ states having $1\sigma^2 2\sigma^2 1\pi^4 1\delta^2 2\pi^1$ and $1\sigma^2 2\sigma^2 1\pi^3 3\sigma^2 1\delta^2$ configurations. These have longer bonds (1.70 and 1.84 Å, respectively) and lie 1.97 and 4.92 eV above the ground state. At a somewhat lower level of theory, B3LYP/HW/6-31G(d), Bohme and co-workers [41] found the $^4\Sigma^-$, $^2\Sigma^-$, and $^4\Pi$ states with excitation energies, 0.0, 0.8, and 2.0 eV, respectively, that agree nicely with those calculated here.

The calculated metal oxide cation bond energies (Table 2) are in good agreement with the experimental values. For HfO^+, these range from 7.04 (CCSD) to 7.54 (QCISD(T)) eV versus 6.91 ± 0.11 eV; for TaO^+, 7.22 (CCSD) to 7.84 (QCISD(T)) eV versus 7.10 ± 0.12 eV; and for WO^+, 6.60 (CCSD) to 7.11 (QCISD(T)) eV versus 6.77 ± 0.07 eV. Except for the CCSD result for WO^+, the computed bond energies are systematically higher than our experimental values, with mean absolute deviations (MADs) of only 0.14, 0.16, and 0.21 eV for CCSD, QCISD, and B3LYP values, respectively, somewhat larger than the experimental uncertainties. Addition of perturbative triple excitations, CCSD(T) and QCISD(T), increases the MADs for the three oxides somewhat to 0.48 and 0.57 eV, respectively. It should be realized that spin–orbit effects are not included in these theoretical values. Specifically, the 0 K experimental numbers should correspond to dissociation to the lowest spin–orbit state of the metal ion, whereas the theoretical numbers correlate with the average of all spin–orbit levels of the ground state of the metal ion (differences of 0.227, 0.466, and 0.514 eV for Hf^+, Ta^+, and W^+, respectively). However, correcting the theoretical BDEs by subtracting these excitation energies ignores spin–orbit coupling in the metal oxide ions, which

has been calculated to be as much as 0.56 eV for the TaC^+ molecule [48].

No matter the exact values, the experimental and theoretical BDEs clearly follow the same trends, i.e., $D(TaO^+) > D(HfO^+) > D(WO^+)$, with only small variations in the three values. This is consistent with the ground state electronic configurations of the three species, $^2\Sigma^+$ ($1\sigma^2 2\sigma^2 1\pi^4 3\sigma^1$), $^3\Delta$ ($1\sigma^2 2\sigma^2 1\pi^4 3\sigma^1 1\delta^1$), and $^4\Sigma^-$ ($1\sigma^2 2\sigma^2 1\pi^4 3\sigma^1 1\delta^2$), respectively, which all have a bond order of three and differ only in the occupation of the nonbonding 3σ and 1δ orbitals. Furthermore, coupling atomic O (^{3}P, $2s^2 2p^4$) with the ground state electronic configurations of the atomic metal ions, Ta^+ (^{5}F, $6s^1 5d^3$) and W^+ (^{6}D, $6s^1 5d^4$), leads directly to the ground states of TaO^+ and WO^+. However, Hf^+ (^{2}D, $6s^2 5d^1$) must promote to the ^{4}F ($6s^1 5d^2$) state lying 0.56 eV (average of all spin–orbit levels) above the ^{2}D state [68], which probably explains why the bond energy for HfO^+ is slightly weaker than that for TaO^+.

5.3. Theoretical results: Metal carbide cations

Qualitatively, the bonding in transition metal carbides should parallel that for the oxides fairly closely. The same valence orbitals are available, with two less valence electrons. For HfC^+, there are seven valence electrons, suggesting a ground state electron configuration of $1\sigma^2 2\sigma^2 1\pi^3$ ($^2\Pi$) or $1\sigma^2 2\sigma^1 1\pi^4$ ($^2\Sigma^+$). The present calculation finds the latter is the ground state ($r = 1.784$ Å), indicating that configuration interaction has moved the 2σ orbital above the 1π orbitals. Indeed, no state corresponding to the predicted $^2\Pi$ was ever located theoretically, although there are a multitude of low-lying excited states (Table S2). In most cases, an electron is removed from the 1π bonding orbital of the ground state leading to a longer bond length, $r > 1.90$ Å. Formation of the $^2\Sigma^+$ ($1\sigma^2 2\sigma^1 1\pi^4$) ground state cannot be achieved by diabatic coupling of atomic C (^{3}P, $2s^2 2p^2$) with the ground state of Hf^+ (^{2}D, $6s^2 5d^1$), but instead requires the Hf^+ (^{4}F, $6s^1 5d^2$) state lying 0.56 eV higher in energy (average of all spin–orbit levels) [68].

The TaC^+ molecule has been theoretically studied before by Majumdar and Balasubramanian (MB) [48] using the CASMCSCF level of theory followed by spin–orbit configuration interaction calculations. They find four low-lying states, $^1\Sigma^+$ ($1\sigma^2 2\sigma^2 1\pi^4$), $^3\Sigma^+$ ($1\sigma^2 2\sigma^1 1\pi^4 3\sigma^1$), $^3\Delta$ ($1\sigma^2 2\sigma^1 1\pi^4 1\delta^1$), and $^1\Delta$ ($1\sigma^2 2\sigma^1 1\pi^4 1\delta^1$), corresponding to adding a 2σ, 3σ, 1δ, and 1δ electron, respectively, to the ground state configuration of HfC^+. These states have relative energies of 0.0, 0.03, 0.43, and 0.51 eV, respectively, and are not greatly influenced by spin–orbit corrections. Bond lengths are 1.731, 1.739, 1.760, and 1.816 Å, respectively. Our B3LYP results are roughly similar with excitation energies for these states of 0.0, 0.08, 0.37, and 0.41 eV, respectively, and bond lengths of 1.718, 1.751, 1.747, and 1.758 Å. The 0 K adiabatic bond energy calculated by MB for their $^1\Sigma^+$ ground state was 4.50 eV (adjusted for the excited state asymptote used in the diabatic bond energy cited by MB), whereas our 0 K BDEs range from 4.32 to 4.88 eV (Table 2). It should be noted that there were some difficulties in the present single configuration calculations of the $^1\Sigma^+$ state, which can be attributed to mixing between $1\sigma^2 2\sigma^2 1\pi^4$ and $1\sigma^2 2\sigma^1 1\pi^4 3\sigma^1$ configurations and some spin contamination as a result of mixing with the low-lying $^3\Sigma^+$ state. At first glance, it seems odd that the $^1\Sigma^+$ state, which has a bond order of three, is not much lower in energy than the $^3\Sigma^+$, $^3\Delta$, and $^1\Delta$ states, which all have one less sigma bonding electron (bond order of 2.5). This is because the latter three states diabatically correlate with the Ta^+ (^{5}F, $6s^1 5d^3$) + C (^{3}P, $2s^2 2p^2$) ground state asymptote, whereas the $^1\Sigma^+$ state diabatically correlates with the Ta^+ (^{3}F, $6s^2 5d^2$) + C (^{3}P, $2s^2 2p^2$) asymptote, lying 0.43 eV higher in energy (average of all spin–orbit levels) [68].

For WC^+, the ground state is $^2\Delta$ ($1\sigma^2 2\sigma^2 1\pi^4 1\delta^1$), consistent with the qualitative bonding picture developed above. This has a short bond length of 1.687 Å, whereas most excited states have bond lengths in excess of 1.72 Å (Table S2). This can be attributed to the fact that these states involve moving an electron from the 2σ bonding orbital into a nonbonding orbital. Nevertheless, the excitation energies are modest, ranging from 0.32 to 1.16 eV (Table S2). The ground state configuration cannot be achieved by coupling atomic C (^{3}P, $2s^2 2p^2$) with the ground state of W^+ (^{6}D, $6s^1 5d^4$), a combination that leads to the $^4\Delta$ ($1\sigma^2 2\sigma^1 1\pi^4 3\sigma^1 1\delta^1$) and $^4\Sigma^-$ ($1\sigma^2 2\sigma^1 1\pi^4 1\delta^2$) excited states, among others. Instead, the $^2\Delta$ state correlates diabatically with W^+ (^{4}F, $6s^1 5d^4$), lying 1.074 eV higher in energy (average of all spin–orbit levels) [68].

For the carbides, the calculated and experimental BDEs do not agree as well as for the oxides (Table 2). The calculated BDEs for HfC^+, TaC^+, and WC^+ range from 3.25 (CCSD) to 3.67 (B3LYP), 4.32 (CCSD) to 4.88 (CCSD(T)), and 4.34 (QCISD(T)) to 4.88 (B3LYP) eV, respectively, compared to the experimental values of 3.19 ± 0.03, 3.79 ± 0.04, and 4.76 ± 0.09 eV, respectively. Again the theoretical values tend to lie above the experimental BDEs, with discrepancies generally a little larger than the oxides. Nevertheless the trends in the BDEs are similar in both the experimental and theoretical values. The calculated ground state electronic configurations of the three species, $^2\Sigma^+$ ($1\sigma^2 2\sigma^1 1\pi^4$), $^1\Sigma^+$ ($1\sigma^2 2\sigma^2 1\pi^4$), and $^2\Delta$ ($1\sigma^2 2\sigma^2 1\pi^4 1\delta^1$), respectively, have bond orders of 2.5, 3, and 3, which would suggest that the bond energies should be more comparable to those of the oxides. Instead, we note that the ratio of the WC^+ and WO^+ BDEs is approximately 2/3, suggesting that the carbide has only a double bond, which in turn indicates that the 2σ orbital is not strongly bonding. The earlier metal carbide cations of hafnium and tantalum have even weaker BDEs, which is at least partially attributable to the promotion energy arguments noted above.

5.4. Potential energy surfaces for CO activation

For the activation of CO ($^1\Sigma^+$) by all three metal cations, the first step is to form a MCO^+ intermediate having a linear, end-on structure. The observation of both MC^+ and MO^+ products suggests that activation of the CO bond has occurred to form a C–M^+–O intermediate at elevated energies. Calculated potential energy surfaces for these systems are shown in Fig. 4. Table S3 lists the geometries and energies of various stable states of the MCO^+ and CMO^+ species for all three metals calculated at the B3LYP/HW+/6-311+G(3df) level of theory.

Interaction of CO ($^1\Sigma^+$) with Hf^+(^{2}D) forms a $HfCO^+$ ($^4\Sigma^-$) intermediate having a linear, end-on structure at 1.12 eV below the reactants. Although formation of this complex is spin-forbidden, several excited states of this complex (including doublet spin states) are found to lie from 0.14 ($^2\Sigma^-$) to 5.21 ($^4\Pi$) eV higher in energy (Table S3). There are also several stable geometries in which the CO ligand is bound side-on, such that the C–Hf–O bond angle is near 30° (Table S3). The lowest of these is a $^4A''$ state lying 0.87 eV above $HfCO^+$ ($^4\Sigma^-$). Calculations indicate that the inserted $CHfO^+$ species has a $^4A''$ ground state that lies in a shallow well 1.32 eV above the ground state reactants (Fig. 4a). Thus, the calculations indicate that the HfC^+ and HfO^+ bonds are much stronger than the analogues in $CHfO^+$, a result that is not surprising as electron density must be shared in the two ligand complex. Excited $^2A''$, $^2A'$, and $^4A'$ states of the $CHfO^+$ species were also found lying 0.29, 1.08, and 2.68 eV higher in energy, respectively. Note that the $^4A'$ state has the longest Hf—O bond but the shortest Hf—C bond, whereas the $^2A'$ state has the reverse (Table S3). $HfC^+ + O$ and $HfO^+ + C$ products can be formed from the C–Hf^+–O intermediates and have experimental

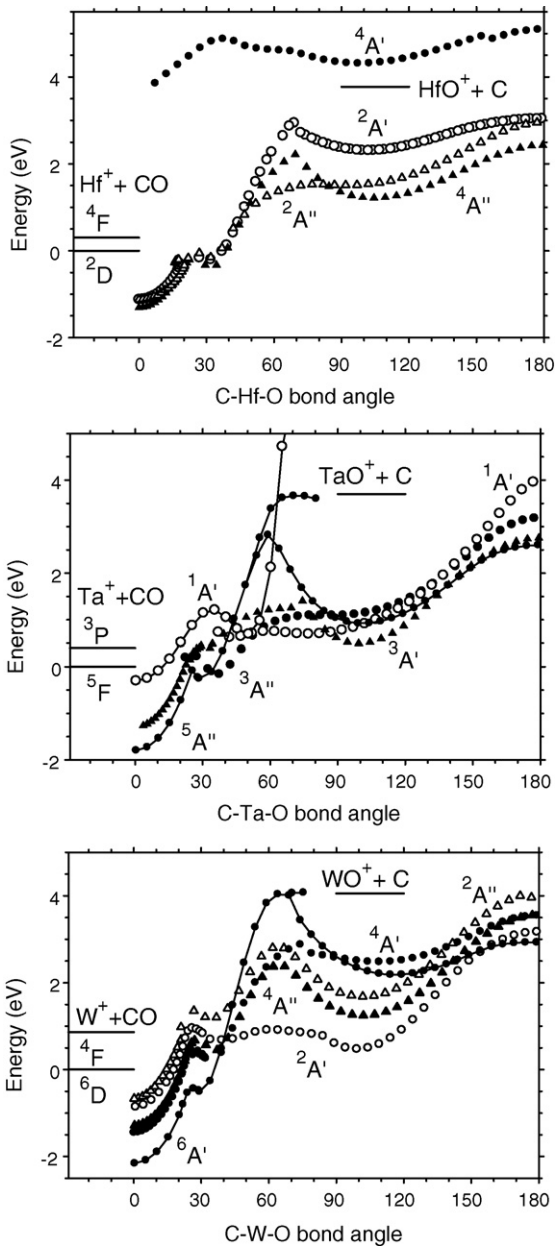

Fig. 4. Representative relaxed potential energy surface scans of the bond angle in the MCO^+ systems calculated at the B3LYP/HW+/6-311+G(3df) level without zero point energy corrections. Circles and triangles represent surfaces of A′ and A″ symmetry, respectively. Calculated energies of reactant ($M^+ + CO$) and product ($MO^+ + C$) asymptotes are indicated by horizontal bars to the left and middle, respectively.

endothermicities of 7.92 ± 0.03 eV and 4.20 ± 0.11 eV, respectively, relative to the entrance channel of $Hf^+ + CO$. The calculated potential energy surfaces (Fig. 4a) indicate that there are no barriers along the reaction paths in excess of the endothermicities of the reactions, which suggests that the thresholds measured experimentally should correspond to the thermodynamics of the product asymptotes, yielding accurate HfC^+ and HfO^+ bond energies.

Interaction of CO ($^1\Sigma^+$) with Ta^+(^{5}F) initially forms a $TaCO^+$($^5\Delta$) intermediate having a linear, end-on structure at 1.74 eV below the reactants. This species has several excited states ranging from 0.50 ($^1\Sigma^+$) to 2.14 ($^1\Sigma$) eV higher in energy (Table S3). The lowest energy side-on complex is a ^{5}A″ that lies 0.24 eV below reactants (Table S3). Calculations indicate that the inserted $CTaO^+$ species has a ^{3}A′ ground state that lies in a shallow well 0.49 eV above the reactants (Fig. 4b). Again because electron density must be shared in the two ligand complex, the bonds in $CTaO^+$ are weaker than in isolated TaC^+ and TaO^+ molecules. Excited ^{1}A′, ^{3}A″, ^{5}A′, and ^{5}A″ states of $CTaO^+$ were also found lying 0.19, 0.50, 3.14, and 4.02 eV higher in energy, respectively (Table S3). $TaC^+ + O$ and $TaO^+ + C$ products can be formed from the C–Ta^+–O intermediates and have experimental endothermicities of 7.32 ± 0.04 and 4.01 ± 0.12 eV, respectively, relative to the ground state entrance channel of Ta^+ (^{5}F) + CO. As for the hafnium system, no barriers along the reaction paths in excess of the endothermicities of the reactions (Fig. 4b) indicate that accurate thermodynamic information about the TaC^+ and TaO^+ products can be obtained from the present threshold measurements.

W^+(^{6}D) interacts with CO ($^1\Sigma^+$) to form a WCO^+($^6\Sigma^+$) intermediate having a linear, end-on structure at 2.09 eV below the reactants. Excited states of this species were also found ranging from 0.71 ($^4\Phi$) to 3.91 ($^6\Pi$) eV higher in energy (Table S3). Side-on complexes were also located and lie 0.49 eV below the reactants (^{6}A′) to 1.00 eV above (^{2}A″) (Table S3). Calculations indicate that the inserted CWO^+ species has a ^{2}A′ ground state that lies in a shallow well 0.47 eV above the reactants (Fig. 4c). Thus, the calculations indicate that the WC^+ and WO^+ bonds are much stronger than the analogues in CWO^+, again a result of sharing the bonding electrons on tungsten with both ligands. Excited ^{4}A′, ^{4}A″, ^{2}A″, ^{6}A′, and ^{6}A″ states of the CWO^+ intermediate were also found lying 0.28, 0.76, 1.20, 1.69, and 3.75 eV higher in energy, respectively (Table S3). It is found that the W—O bond length is roughly the same in all four states, whereas the W—C bond length tracks with increasing energy above the reactants (Table S3). $WC^+ + O$ and $WO^+ + C$ products can be formed from the C–W^+–O intermediates and have endothermicities of 6.35 ± 0.09 and 4.34 ± 0.07 eV, respectively, relative to the ground state entrance channel of $W^+ + CO$. No barriers along the reaction paths in excess of the endothermicities of the reactions are found (Fig. 4c), which means that the thresholds should correspond to the asymptotic energies of the products for both reactions.

The results for the potential energy surface in the tungsten system are in qualitatively good agreement with previous theoretical results on WCO^+ obtained by Musaev et al. [56], who calculated the lowest energy linear, side-on, and inserted species of sextet, quartet, and doublet spin. We find that the CWO^+ (^{2}A′) insertion species lies 2.57 eV above the linear WCO^+($^6\Sigma^+$) ground state species compared to 3.00 calculated by Musaev et al. These authors also calculated that the lowest lying quartet and doublet states (symmetries unspecified) lie above the sextet state of WCO^+ by 1.32 and 2.65 eV, respectively, compared to 0.71 and 1.30 eV, respectively, found here.

We did not explore the potential energy surface corresponding to approach of the metal cations with the oxygen end of the carbon monoxide molecule. The MOC^+ intermediates are anticipated to be much less stable than the corresponding MCO^+ species and could easily collapse to the side-on species identified above.

6. Summary

In this study, we are able to generate Hf^+, Ta^+, and W^+ ions in their ground states by using a direct current discharge/flow tube (DC/FT) ion source. Corresponding state-specific cross sections for these ions with O_2 and CO are obtained. The former reactions are all exothermic, whereas analyses of the endothermic reaction cross sections for the latter systems yield BDEs for the metal oxide and carbide cations listed in Table 2. These values include the first thermodynamic values for HfC^+ and TaC^+ and improved thermochemistry for WC^+ and the three metal oxide cations. In Table 3, the cationic BDEs for the oxides are combined with heats of formation of the neutral species taken from the literature to derive improved ionization energies of the neutral metal oxides, or in the case of TaO

and WO where the IE values are well determined, alternate values for the neutral heats of formation.

Detailed quantum calculations were also performed for the metal carbide and oxide diatoms examined experimentally. The nature of the bonding in MO^+ and MC^+ is analyzed using theoretical calculations at a B3LYP/HW+/6-311+G(3df) level of theory. Bond energies for all MO^+ and MC^+ species are calculated using geometries calculated at this level and single point energies determined at B3LYP, CCSD, CCSD(T), QCISD, and QCISD(T) levels of theory with the same basis set. Reasonable agreement between the theoretical and experimental bond energies for the three metal oxide and three metal carbide cations is found. Potential energy surfaces for reaction of the metal cations with CO are also calculated at the B3LYP/HW+/6-311+G(3df) level of theory and demonstrate that the reactions occur by insertion of the metal cation into the CO bond followed by loss of either the C or O neutral atom product, with no barriers in excess of the endothermicity.

Acknowledgement

This work is supported by the National Science Foundation, grant no. CHE-0748790.

Appendix A. Supplementary data

Supplementary data associated with this article can be found, in the online version, at doi:10.1016/j.ijms.2008.08.025.

References

[1] E.K. Stroms, in: J.L. Margrave (Ed.), Refractory Materials, vol. 2, Academic Press, New York, 1967.
[2] H. Silberbach, H.Z. Merz, Physica B 59 (1985) 143.
[3] K. Gesheva, E. Vlakhov, Mater. Lett. 5 (1987) 276.
[4] D. Smith, N.G. Adams, Plasma Chemistry I, Vol. 89 of Topics in Current Chemistry, Springer-Verlag, Berlin, 1980, p. 1.
[5] E. Murad, J. Geophys. Res. 83 (1978) 5525;
Tech. Rep. AFGL-TR-77-0235, Air Force Geophysics Laboratory, Hanscom Air Force Base, MA, 1977.
[6] R.A. Sheldon, in: D.H. Barton, A.E. Martell, D.T. Sawyer (Eds.), The Activation of Dioxygen and Homogeneous Catalytic Oxidation, Plenum, New York, 1993, p. 9;
R.A. Sheldon, J.K. Kochi, Metal-Catalyzed Oxidations of Organic Compounds, Academic, New York, 1981.
[7] S.K. Loh, E.R. Fisher, L. Lian, R.H. Schultz, P.B. Armentrout, J. Phys. Chem. 93 (1989) 3159.
[8] E.R. Fisher, J.L. Elkind, D.E. Clemmer, R. Georgiadis, S.K. Loh, N. Aristov, L.S. Sunderlin, P.B. Armentrout, J. Chem. Phys. 93 (1990) 2676.
[9] S.K. Loh, L. Lian, P.B. Armentrout, J. Chem. Phys. 91 (1989) 6148.
[10] Y.–M. Chen, P.B. Armentrout, J. Chem. Phys. 103 (1995) 618.
[11] M.R. Sievers, Y.-M. Chen, P.B. Armentrout, J. Chem. Phys. 105 (1996) 6322.
[12] X.-G. Zhang, P.B. Armentrout, J. Phys. Chem. A 107 (2003) 8904.
[13] K.P. Huber, G. Herzberg, Molecular Spectra and Molecular Structure. IV. Constants of Diatomic Molecules, Van Nostrand Reinhold, New York, 1979.
[14] M.B. Panish, L.J. Reif, Chem. Phys. 38 (1963) 253.
[15] R.J. Ackermann, E.G. Rauh, J. Chem. Phys. 60 (1974) 2266.
[16] J.B. Pedley, E.M. Marshall, J. Phys. Chem. Ref. Data 12 (1983) 967.
[17] J.B. Bhartiya, S.H. Behere, Curr. Sci. 55 (1986) 383.
[18] E.G. Rauh, R.J. Ackermann, J. Chem. Phys. 60 (1974) 1396.
[19] C.L. Callender, P.A. Hackett, D.M. Rayner, J. Opt. Soc. Am. B 5 (1988) 1341.
[20] D. Schroder, H. Schwarz, S. Shaik, Struct. Bond. 97 (2000) 91.
[21] S.G. Lias, J.E. Bartmess, J.F. Liebman, J.L. Holmes, R.D. Levin, W.G. Mallard, J. Phys. Chem. Ref. Data 17 (Suppl. 1) (1988) 1.
[22] R.J. Vanzee, S. Li, W. Weltner, Chem. Phys. Lett. 217 (1994) 381.
[23] A. Hansson, A. Pettersson, P. Royen, U. Sassenberg, J. Mol. Spectrosc. 224 (2004) 157.
[24] R.S. Ram, P.F. Bernath, J. Mol. Spectrosc. 169 (1995) 268.
[25] L.A. Kaledin, J.E. McCord, M.C. Heaven, J. Mol. Spectrosc. 173 (1995) 37.
[26] M.W. Chase, Jr., J. Phys. Chem. Ref. Data, Monograph No. 9 (1963) 1.
[27] M.G. Inghram, W.A. Chupka, J. Berkowitz, J. Chem. Phys. 27 (1957) 569.
[28] O.H. Krikorian, J.H. Carpenter, J. Phys. Chem. 69 (1965) 4399.
[29] J. Drowart, A. Pattoret, S. Smoes, F. Degreve, D. Detry, in: W.L. Mead (Ed.), Advances in Mass Spectrometry, vol. 3, Inst. Petroleum, London, 1966, p. 931.
[30] S. Smoes, J. Drowart, C.E. Myers, J. Chem. Thermodyn. 8 (1976) 225.
[31] J.M. Dyke, A.M. Ellis, M. Feher, A. Morris, A.J. Paul, J.C.H. Stevens, J. Chem. Soc. Faraday Trans. 2 83 (1987) 1555.
[32] R.J. Ackermann, E.G. Rauh, R.J. Thorn, J. Chem. Phys. 65 (1976) 1027.
[33] B. Simard, P. Kowalczyk, A.M. James, Phys. Rev. 50 (1994) 846.
[34] W. Weltner, D. McLeod, J. Chem. Phys. 42 (1965) 882.
[35] C.J. Cheetham, R.F. Barrow, Trans. Faraday Soc. 63 (1967) 1835.
[36] R.S. Ram, P.F. Bernath, J. Mol. Spectrosc. 191 (1998) 125.
[37] A. Al-Khalili, U. Hallsten, O. Launila, J. Mol. Spectrosc. 198 (1999) 230.
[38] K.J. Manke, T.R. Vervoort, K.T. Kuwata, T.D. Varberg, J. Chem. Phys. 128 (2008) 104302.
[39] W.J. Zheng, X. Li, S. Eustis, K. Bowen, Chem. Phys. Lett. 460 (2008) 68.
[40] G. DeMaria, R.P. Burns, J. Drowart, M.G. Inghram, J. Chem. Phys. 32 (1960) 1373.
[41] V. Blagojevic, G.K. Koyanagi, V.V. Lavrov, G. Orlova, D.K. Bohme, Chem. Phys. Lett. 389 (2004) 303.
[42] M.D. Campbell-Miller, B. Simard, J. Opt. Soc. Am. B 13 (1996) 2115.
[43] R.S. Ram, J. Lievin, G. Li, T. Hirao, P.F. Bernath, Chem. Phys. Lett. 343 (2001) 437.
[44] M. Lorenz, V.E. Bondybey, Chem. Phys. 241 (1999) 127.
[45] M.W. Heaven, G.M. Stewart, M.A. Buntine, G.F. Metha, J. Phys. Chem. A 104 (2000) 3308.
[46] C.J. Cassady, S.W. McElvany, J. Phys. Chem. 94 (1990) 2057.
[47] C.J. Cassady, S.W. McElvany, J. Am. Chem. Soc. 112 (1990) 4188.
[48] D. Majumdar, K. Balasubramanian, Chem. Phys. Lett. 294 (1998) 273.
[49] K. Balasubramanian, J. Chem. Phys. 112 (2000) 7425.
[50] S.M. Sickafoose, A.W. Smith, M.D. Morse, J. Chem. Phys. 116 (2002) 993.
[51] X. Li, S.S. Liu, W. Chen, L.-S. Wang, J. Chem. Phys. 111 (1999) 2464.
[52] P.B. Armentrout, S. Shin, R. Liyanage, J. Phys. Chem. A 110 (2006) 1242.
[53] R.E. Winters, R.W. Kiser, Inorg. Chem. 4 (1965) 157.
[54] F. Qi, L. Sheng, H. Gao, Y. Zhang, X. Yang, S. Yang, S. Yu, Huaxue Wuli Xuebao 12 (1999) 525.
[55] F. Qi, S. Yang, L. Sheng, H. Gao, Y. Zhang, S. Yu, J. Chem. Phys. 107 (1997) 10391.
[56] D.G. Musaev, S. Irle, M.C. Lin, J. Phys. Chem. A 111 (2007) 6665.
[57] S.K. Loh, D.A. Hales, L. Lian, P.B. Armentrout, J. Chem. Phys. 90 (1989) 5466.
[58] R.H. Schultz, P.B. Armentrout, Int. J. Mass Spectrom. Ion Process. 107 (1991) 29.
[59] E. Teloy, D. Gerlich, Chem. Phys. 4 (1974) 417;
D. Gerlich, in: C.-Y. Ng, M. Baer (Eds.), State-Selected and State-to-State Ion-Molecule Reaction Dynamics. Part I. Experiment, vol. 82, Wiley, New York, 1992, p. 1 (Adv. Chem. Phys.).
[60] K.M. Ervin, P.B. Armentrout, J. Chem. Phys. 83 (1985) 166.
[61] P.J. Chantry, J. Chem. Phys. 55 (1971) 2746.
[62] B.L. Kickel, P.B. Armentrout, J. Am. Chem. Soc. 117 (1995) 4057.
[63] D.E. Clemmer, Y.-M. Chen, F.A. Khan, P.B. Armentrout, J. Phys. Chem. 98 (1994) 6522.
[64] C.L. Haynes, P.B. Armentrout, Organometallics 13 (1994) 3480.
[65] B.L. Kickel, P.B. Armentrout, J. Am. Chem. Soc. 117 (1995) 764.
[66] Y.-M. Chen, J.L. Elkind, P.B. Armentrout, J. Phys. Chem. 99 (1995) 10438.
[67] M.R. Sievers, Y.-M. Chen, P.B. Armentrout, J. Phys. Chem. 100 (1996) 54.
[68] C.E. Moore, Atomic Energy Levels, Natl. Bur. Stand. (U.S.) Circ. 467. Vol. III (1958), reprinted as Natl. Stand. Ref. Data Ser., Natl. Bur. Stand. (U.S.) 35 (1971).
[69] C.C. Kiess, J. Res. Natl. Bur. Stand. (U.S.) 66A (1962) 111.
[70] J.O. Ekberg, R. Kling, W. Mende, Phys. Scr. 61 (2000) 146.
[71] P.B. Armentrout, Int. J. Mass Spectrom. 200 (2000) 219.
[72] W.J. Chesnavich, M.T. Bowers, J. Phys. Chem. 83 (1979) 900.
[73] P.B. Armentrout, in: N.G. Adams, L.M. Babcock (Eds.), Advances in Gas Phase Ion Chemistry, 1, JAI, Greenwich, 1992, p. 83.
[74] F. Muntean, P.B. Armentrout, J. Chem. Phys. 115 (2001) 1213.
[75] M.E. Weber, J.L. Elkind, P.B. Armentrout, J. Chem. Phys. 84 (1986) 1521.
[76] A.D. Becke, J. Chem. Phys. 98 (1993) 5648.
[77] C. Lee, W. Yang, R.G. Parr, Phys. Rev. B 37 (1988) 785.
[78] Gaussian 03, Revision B.02, M.J. Frisch, G.W. Trucks, H.B. Schlegel, G.E. Scuseria, M.A. Robb, J.R. Cheeseman, J.A. Montgomery, Jr., T. Vreven, K.N. Kudin, J.C. Burant, J.M. Millam, S.S. Iyengar, J. Tomasi, V. Barone, B. Mennucci, M. Cossi, G. Scalmani, N. Rega, G.A. Petersson, H. Nakatsuji, M. Hada, M. Ehara, K. Toyota, R. Fukuda, J. Hasegawa, M. Ishida, T. Nakajima, Y. Honda, O. Kitao, H. Nakai, M. Klene, X. Li, J.E. Knox, H.P. Hratchian, J.B. Cross, V. Bakken, C. Adamo, J. Jaramillo, R. Gomperts, R.E. Stratmann, O. Yazyev, A.J. Austin, R. Cammi, C. Pomelli, J.W. Ochterski, P.Y. Ayala, K. Morokuma, G.A. Voth, P. Salvador, J.J. Dannenberg, V.G. Zakrzewski, S. Dapprich, A.D. Daniels, M.C. Strain, O. Farkas, D.K. Malick, A.D. Rabuck, K. Raghavachari, J.B. Foresman, J.V. Ortiz, Q. Cui, A.G. Baboul, S. Clifford, J. Cioslowski, B.B. Stefanov, G. Liu, A. Liashenko, P. Piskorz, I. Komaromi, R. L. Martin, D.J. Fox, T. Keith, M.A. Al-Laham, C.Y. Peng, A. Nanayakkara, M. Challacombe, P.M.W. Gill, B. Johnson, W. Chen, M.W. Wong, C. Gonzalez, J.A. Pople, Gaussian, Inc., Wallingford CT, 2004.
[79] P.J. Hay, W.R. Wadt, J. Chem. Phys. 82 (1985) 299.
[80] G. Ohanessian, M.J. Brusich, W.A. Goddard III, J. Am. Chem. Soc. 112 (1990) 7179.
[81] J.B. Foresman, A.E. Frisch, Exploring Chemistry with Electronic Structure Methods, Gaussian, Inc., Pittsburgh, PA, 1996.
[82] G. Gioumousis, D.P. Stevenson, J. Chem. Phys. 29 (1958) 294.
[83] E.W. Rothe, R.B. Bernstein, J. Chem. Phys. 31 (1959) 1619.
[84] G.K. Koyanagi, D. Caraiman, V. Blagojevic, D.K. Bohme, J. Phys. Chem. A 106 (2002) 4581.
[85] N. Aristov, P.B. Armentrout, J. Phys. Chem. 91 (1987) 6178.
[86] J.D. Burley, K.M. Ervin, P.B. Armentrout, Int. J. Mass Spectrom. Ion Process. 80 (1987) 153.
[87] T.M. Miller, B. Bederson, Adv. Atom. Mol. Phys. 13 (1977) 1.